Article

Photoprotective archaeosomes made of lipids extracted with bio-solvents.

Yamila Roxana Simioni , Victoria Rebeca Dana Gonzalez Epelboim , Gustavo Apezteguia , Leticia Herminia Higa , Eder Lilia Romero , Maria Jose Morilla *

Posted Date: 12 January 2026

doi: 10.20944/preprints202601.0767.v1

Keywords: archaeal lipids; green extraction; ethyl acetate; ethanol; photoprotection; HaCaT cells

 doi:10.20944/preprints202601.0767.v1

Article

Photoprotective Archaeosomes Made of Lipids Extracted with Bio-Solvents

Yamila Roxana Simioni, Victoria Rebeca Dana Gonzalez Epelboim, Gustavo Apezteguia, Leticia Herminia Higa, Eder Lilia Romero and Maria Jose Morilla *

Centro de investigación y Desarrollo de Nanomedicinas (CIDeN), Departamento de Ciencia y Tecnología, Universidad Nacional de Quilmes, Roque Sáenz Peña 352, B1876 Bernal, Buenos Aires, Argentina

* Correspondence: jmorilla@unq.edu.ar

Abstract

Archaea lipids are a source of new biomaterials for pharmaceutical and nanomedical applications; however, their classic extraction method relies on chloroform and methanol, toxic solvents that conflict with green chemistry principles. In this paper we explore the performance of an eco-friendly method for the extraction of total lipids from the haloarchaea *Halorubrum tebenquichense.* Using the bio-solvents ethyl acetate and ethanol in a two-step procedure, a fraction of total lipids (135 ± 41 mg phospholipids and 1.1 ± 0.4 mg bacterioruberin (BR) / 100 g cell paste) was obtained containing the same composition as that resulting from extraction with the classical solvents as confirmed by Electrospray Ionization Mass Spectrometry, although with lower phospholipid content, thus with a higher proportion of bacterioruberin. The extracted lipids were subsequently utilized for preparation of archaeosomes, which were characterized by uniform size distribution (406 ± 137 nm, 0.63 ± 0.13 polydispersity index), colloidal stability, and negative ζ potential (-38.2 ± 5.4 mV). The photoprotective potential of these archaeosomes was for the first time determined in human keratinocyte (HaCaT) cells exposed to UVB irradiation (270 mJ/cm^2). Treatment with archaeosomes significantly ($p< 0.05$) enhanced cell viability (from ~43 to ~80 %), reduced intracellular ROS generation and proinflammatory cytokine release (TNF-α) and mitigated UVB-induced apoptosis compared to untreated controls, indicating effective cytoprotection. This study demonstrates that ethyl acetate–ethanol-based extraction offers an alternative for archaeal lipid recovery and highlights the potential of archaeosomes as natural photoprotective agents for skincare applications.

Keywords: archaeal lipids; green extraction; ethyl acetate; ethanol; photoprotection; HaCaT cells

1. Introduction

Haloarchaea thrive in hypersaline environments (20–30% w/v NaCl) and are exposed to intense solar radiation, relying on a suite of molecular and physiological adaptations that maintain osmotic balance, stabilize proteins, and protect cellular structures. Their membranes are composed of both polar polyisoprenoid diethers (polar archaeolipids, PA) and neutral lipids (NA) [1]. PA constitute unique biomaterials that are clearly distinguished from bacterial and eukaryotic lipids by their glycerol-1-phosphate backbone and ether-linked isoprenoid chains [2,3]. Their stereoisomerism, ether linkages, and saturated isoprenoid chains endow them with exceptional resistance to chemical degradation (including ester bond hydrolysis and oxidation of unsaturated fatty acids), physical destabilization (aggregation and fusion), and environmental stresses such as pH, temperature, and enzymatic attack [4–6]. On the other hand, bacterioruberin (BR), a C50 xanthophyll with 13 conjugated double bonds and 4 hydroxyl groups represents between 51 and 81 % (and up to 95 % in highly pigmented strains) of NA [7]. BR fulfils multiple biological roles, notably providing protection against UV radiation and enhancing membrane hydrophobicity, thereby reducing intracellular water loss while promoting the passive diffusion of oxygen molecules across the cell membrane [8,9],

 doi:10.20944/preprints202601.0767.v1

Besides, BR production is typically induced under stress conditions such as high salinity, intense light and oxidative stress [10–13].

Archaeosomes (ARC), nanovesicles made with PA from halophilic archaea *Halorubrum tebenquichense* are acknowledged as colloidally and chemically resistant to heat sterilization, storage under cold-free conditions [14], nebulization [15] and gastrointestinal digestion [16,17]. Besides, achaeosomes of different composition have shown to be bioactive, for instance ARC made with PA and cholesterol show endothelial anti-inflammatory properties [18]. Besides, ARC made by mixing different amounts of PA and NA show anti-inflammatory activity on lipopolysaccharide or H_2O_2-stimulated macrophages [19].

Classically, total archaeolipids (TA) consisting of the mixture of PA and NA, are isolated from halophilic archaea by sequential extraction steps based on a modified Bligh–Dyer method specifically adapted for extreme halophiles [16,20–22]. This method employs chloroform and methanol, well-documented toxicological and environmental hazards [23,24], regulated as hazardous waste, resulting in high disposal costs [25–27]. Methanol is additionally classified as a highly volatile and flammable solvent [24].

The bio-solvents (green solvents produced from natural resources) ethanol (EtOH, as a substitute for methanol) and ethyl acetate (EtOAc, as a substitute for chloroform) has been used as effective alternative to classical solvents for extracting total lipids from yeast biomass in terms of yield and selectivity [28,29]. Both solvents are approved for use in the manufacture of food ingredients and cosmetic products—for example, EtOAc is common in nail polish removers, while EtOH is widely used in perfumes, lotions, and hair- and skincare formulations [30]. Both solvents also exhibit low environmental impact and are relatively easy to recycle [31–33]. However, their efficacy in extracting TA from halophilic archaea remains underexplored.

On the other hand, the excessive exposure to UVB (280–320 nm) radiation induces the generation of reactive oxygen species (ROS), lipid peroxidation, DNA damage, and inflammation, ultimately leading to premature skin aging and photo carcinogenesis [34,35]. The search for natural active ingredients with photoprotective activity capable of increasing the antioxidant activity of the skin, reducing levels of inflammation and cell damage is an area of growing interest in dermatology and cosmetics [36,37]. Carotenoids, including β-carotene, and xanthophylls such as astaxanthin and fucoxanthin, are well known for their photoprotective activity [38–40]. However, their intrinsic instability (fast degradation induced by heat, light, oxygen, and catalytic agents), their high lipophilicity, poor aqueous solubility and requirement of organic solvents (e.g., DMSO) for dissolution, restrict their application in conventional pharmaceutical formulations, limiting their topical bioavailability [41]. Enhancing stability, solubility and bioavailability of carotenoids require appropriate formulation strategies, such as incorporation into nanoparticles, which upon cell internalized, also provide efficient intracellular delivery [42,43]. Such last fact is critical to maximize the activity of molecules such as astaxanthin and BR, since their action is exerted once transversely located in cellular lipid bilayers [44,45].

Remarkably, instead of ARC prepared by mixing PA and NA, ARC prepared with TA allows saving extraction steps, minimizing the use of solvents and processing time. ARC prepared with TA (rich in BR and small amounts of astaxanthin and squalene), have recently shown antitumoral activity on A549 cells [22]. In this study, we investigate the photoprotective potential of ARC prepared with TA extracted by green solvents on HaCaT cells exposed to UVB irradiation. We evaluated their effects on cell viability, intracellular ROS generation, and inflammation. This work aims to elucidate the role of archaeolipid-based systems as natural, stable, and effective agents for protecting skin cells against UV-induced damage.

 doi:10.20944/preprints202601.0767.v1

2. Materials and Methods

2.1. Materials

Methylthiazolyltetrazolium bromide (MTT), 2,2-diphenyl-1-picrylhydrazyl (DPPH), 6-Hydroxy-2,5,7,8-tetramethylchroman-2-carboxylic acid (Trolox) and 6-lauroyl-2-dimethylaminonaphthalene Laurdan, were obtained from Sigma-Aldrich, Argentina. L-glutamine, trypsin, penicillin, streptomycin sulfate, Minimal Essential Medium (MEM) were supplied by Gibco, Buenos Aires, Argentina. Hoechst 33342 (Hoechst), CM-H2DCFDA, Lactate Dehydrogenase kit (LDH), Rhodamine, propidium iodide and YO-PRO were purchased from Thermo Fisher Scientific (Massachusetts, USA). Fetal bovine serum (FBS) was sourced from Internegocios Córdoba, Argentina. Tween 80 was provided by Biopack. All other reagents were of analytical grade and were acquired from Anedra, Argentina.

2.2. Archaea Growth

Halophilic archaea *H. tebenquichense* was cultivated in a halophile-specific growth medium [46] using a custom-built 25 L stainless-steel bioreactor at 40 °C under continuous agitation at 600 rpm. After 96 h of cultivation, the cells were collected by centrifugation and stored as cell paste at 4 °C

2.3. Lipids Extraction by Classical Bligh and Dyer Method

Total archaeolipids (TA) were extracted from the cell paste using a modified Bligh and Dyer method adapted for extreme halophiles (BD-TA) [20]. Briefly, 100 g of cell paste were suspended in of saline solution (20% NaCl, 0.4% KCl, and 2% $MgSO_4$, w/v, 160 ml final volume) and mixed with 600 ml of chloroform–methanol (1:2 v/v). After 2 h of stirring at room temperature, the mixture was centrifuged (600 × g, 10 min) to remove debris. The supernatant (~640 ml) was subjected to successive extractions with (340 ml) chloroform–water (1:1 v/v) [final chloroform–methanol–water (1:1:0.9 v/v)] until colorless, and the organic phase containing TA was collected. Solvents were evaporated under reduced pressure at 37 °C and the lipid residue was vacuum-dried to constant weight and stored at –20 °C.

2.4. Lipids Extraction by with Bio-Solvents

TA were extracted from the cell paste using ethanol (EtOH) and ethyl acetate (EtOAc) as bio-solvents (BS) (BS-TA). Briefly, 100 g of cell paste suspended in 160 ml of saline solution was mixed with 600 ml of EtOAc/EtOH (2:1 v/v). After 2 h of stirring at room temperature, the mixture was centrifuged (600 × g, 10 min) to remove debris. The supernatant (~640 ml) was subjected to successive extractions with 960 ml EtOAc/water (2/1 v/v) [EtOAc/EtOH/water (2:0.38:0.9 v/v)]. Solvents were evaporated under reduced pressure at 37 °C and the lipid residue was vacuum-dried to constant weight and stored at –20 °C.

2.5. Phospholipids, Proteins and Sugar Quantification

Phospholipids (PL) were quantified using a colorimetric phosphate microassay [47]. Proteins were quantified by the BCA assay using a commercial kit (Micro BCA™ Protein Assay Kit, Thermo Scientific) after complete disruption of ARC with 5% v/v SDS (30 min incubation at room temperature). Sugars were quantified by colorimetric titration of carbohydrates by the phenol/sulfuric acid method using a glucose solution as a standard [48].

2.6. BR Quantification

UV/visible spectra of TA extracts dissolved in methanol were taken between 300-700 nm. BR concentration was determined by measuring absorbance of the methanolic solution at 490 nm, applying an average mass extinction coefficient of 2660 $mL \cdot mg^{-1} \cdot cm^{-1}$ [49].

 doi:10.20944/preprints202601.0767.v1

2.7. Electrospray Ionization Mass Spectrometry (ESI-MS)

TA extracts were analyzed by ESI-MS in negative and positive-ion modes using a Bruker micrOTOF-QII mass spectrometer equipped with an electrospray ionization source. Samples (5 µl) dissolved in $CHCl_3$:CH_3OH (1:1, v/v) for negative mode or in CH_3OH:HCOOH (1:1, v/v) for positive mode were injected via a loop injection system and transferred to the electrospray ionization interface at 10 µl/min. Ion source conditions included a nebulizing gas (air) flow rate of 4 l min^{-1}, a drying gas (N_2) flow rate of 4 l min^{-1}, a capillary voltage of 4 kV, and mass spectra acquisition over an m/z range of 50–2000 in both positive and negative ionization modes.

2.8. Antioxidant Activity

The antioxidant capacity of TA extracts was assessed by determining their $DPPH^{\bullet+}$ radical scavenging activity, as previously described [50]. Briefly, TA extracts dissolved in methanol (20 µL) were mixed with a methanolic $DPPH^{\bullet+}$ solution (160 µL) in a 96-well microplate. After incubation for 30 min at 37 °C in the dark with continuous agitation (200 rpm), absorbance was recorded at 580 nm using a Cytation 5 Cell Imaging Multi-Mode Reader (BioTek Instruments, VT, USA). A blank control containing only the $DPPH^{\bullet+}$ solution was included. Trolox (2.6–23 µg mL^{-1}) was used to generate the calibration curve. All assays were performed in three independent experiments, each conducted in triplicate.

2.9. Preparation of Archaeosomes

Archaeosomes made of BD-TA (BD-TA-ARC) or BS-TA (BS-TA-ARC) were prepared using the lipid film hydration method. Briefly, 10 mg of BD-TA or BS-TA were dissolved in $CHCl_3$:CH_3OH (1:1, v/v) and transferred to round-bottom U shaped microcentrifuge tubes. Organic solvents were evaporated under a N_2 stream until a thin lipid film was formed. Subsequently, the lipid films were hydrated with 1 ml of 10 mM Tris, pH 7.4, containing 0.9% w/v NaCl (Tris-HCl buffer) under mechanical stirring. Particle size and lamellarity were reduced by sonication in a bath sonicator at room temperature (20 °C) for 60 min at 80 W of ultrasonic power and 40 kHz of frequency.

2.10. Characterization of Archaeosomes

Particle size and ζ potential were determined by dynamic light scattering (DLS) and phase analysis light scattering (PALS), respectively, using a NanoZsizer (Malvern Instruments, Malvern, United Kingdom). Samples were diluted 1:20 v/v in Tris-HCl buffer (50 µl of nanovesicles in 950 µl of Tris-HCl buffer) prior to measurement.

PL and BR were determined as state before (section 2.5 and 2.6).

Raman spectra were collected using i-Raman spectrometers (models BWS415-532 and BWS465-785S; BWTEK, Plainsboro, NJ, USA) equipped with a video microscope (BAC151B) at the Instituto de Investigaciones Fisicoquímicas Teóricas y Aplicadas (INIFTA), Buenos Aires, Argentina. Excitation was carried out at 532 nm, with acquisition times of 500–1000 ms using 2 or 5 accumulations and laser power settings ranging from 25 to 80%. Spectra were acquired over the spectral range of 182–3200 cm^{-1}.

The membrane order and fluidity of BD-TA-ARC and BS-TA-ARC were determined by measuring generalized polarization (GP) and fluorescence anisotropy (FA) using Laurdan, respectively. Laurdan was incorporated into membranes by incubating Laurdan in Tris-HCl buffer solution (at Laurdan: PL 1:500 (for GP) or 1:20 (for FA) molar ratio) with ARC for 30 min in the dark at room temperature.

GP was calculated using the following Equation:

$$GP = \frac{I_{440} - I_{490}}{I_{440} + I_{490}}$$

 doi:10.20944/preprints202601.0767.v1

where I_{440} and I_{490} represent the fluorescence intensities at λ = 440 nm and λ = 490 nm, respectively, obtained from the emission spectrum recorded between 400 and 520 nm using λ = 364 nm (excitation slit width: 5.0 nm; emission slit width: 10.0 nm; scan speed: 100 nm/min).

FA was calculated using spectrofluorometer software according to the following equation:

$$FA = \frac{I_0 - G.I_{90}}{I_0 + 2G.I_{90}}$$

where I_0 and I_{90} represent the fluorescence intensities measured at λ= 440 nm with λ= 364 nm and the excitation polarizer oriented at 0° and 90°, respectively. The correction factor (G) was obtained from the ratio of emission intensities at 0° and 90° with the excitation polarizer set at 90°, after subtracting the contribution of scattered light.

2.11. Cells Line

HaCaT cells were regularly cultured in MEM, supplemented with 10% fetal bovine serum (FBS), 1% antibiotic/antimycotic (penicillin 10,000 U/ml, streptomycin sulfate 10 mg/ml, and amphotericin B 25 µg/ml), and 2 mM L-glutamine, at 37°C in 5% CO_2 and 95% humidity.

2.12. Cytotoxicity of BS-TA-ARC

The cytotoxicity of BS-TA-ARC was determined by the MTT assay. Briefly, cells seeded at a density of 2 x 10^4 cells per well in a 96-well microplate were grown for 24 h at 37°C. The culture medium was then replaced with 100 µl fresh MEM supplemented with 5% FBS containing AM-TA-ARC at 250, 500, 750, and 1000 µg/ml of PL and cells were incubated for 24 h. The supernatant was then removed, and 100 µl of a 0.5 mg/ml MTT solution in MEM without phenol red was added. After the 3-h incubation, the MTT solution was carefully removed. Insoluble formazan crystals were dissolved in 100 µl of dimethyl sulfoxide, and absorbance was measured at 570 nm using a Cytation 5 microplate reader (BioTek Instruments, VT, USA). Cell viability was expressed as a percentage of cells incubated in MEM containing 10% FBS.

2.13. Uptake of BS-TA-ARC

The uptake of Rhodamine PE-labeled BS-TA-ARC (RhPE at 0.4 µg per mg of PL was added to the mixture of lipids) was determined by fluorescence microscopy. Briefly, cells were seeded in 24-well plates at a density of 7.5 x 10^4 cells per well and incubated at 37°C and 5% CO_2 for 24 h. Then, cells were incubated with BS-TA-ARC at 500 µg/ml for 1, 3 and 24 h at 37°C and at 4°C (for surface adsorption). After incubation, cells were washed with PBS, stained with 20 µl of 160 µM Hoechst for 15 min at room temperature and washed again with PBS. PBS was placed and analyzed by fluorescence microscopy in Cytation 5 plate reader using the fluorescence cube YFP for Rhodamine (561/580) and the DAPI cube (358/461) for Hoescht. Fluorescence measured at 4°C was subtracted from that measured at 37 °C.

2.14. UVB Irradiation and Cell Viability Assay

Radiation cytotoxicity was determined by the MTT assay. For this purpose, cells were seeded at a density of 2 x 10^4 cells per well in a 96-well microplate and grown for 24 h at 37°C. Then, the culture medium was replaced by 100 ul of phosphate-buffered saline (PBS) to minimize UV absorption. Cells were then exposed to UVB light from a 25 W Exo Terra Repti GLO 5.0 lamp (peak emission 311 nm) placed at a fixed distance of 10 cm (irradiance of 170 µW/cm^2) from the culture for 0, 15, 20, 45, 60, 75 and 90 min. The total dose (D) in mJ/cm^2 was calculated using the following equation: D = E x t; where E is irradiance and t is exposure time. After irradiation, PBS was replaced with complete medium and cells were incubated for 24 h before evaluating metabolic activity using the MTT assay as stated before (section 2.12). Cell viability was expressed as a percentage relative to non-irradiated controls.

2.15. Photoprotection of BS-TA-ARC

 doi:10.20944/preprints202601.0767.v1

The photoprotective activity of BS-TA-ARC was determined by pre-treatment of HaCaT cell with 500 µg/ml of BS-TA-ARC for 24 h as stated in section 2.12. Then, the culture medium was replaced by 100 µl of PBS and cells were exposed to UVB light for 20 min. After irradiation, PBS was replaced with complete medium and cells were incubated for another 24 h. Then cytotoxicity was measured by the MTT assay on adherent cells (as stated before) and measuring the release of the cytosolic enzyme lactate dehydrogenase (LDH) in the culture medium by LDH activity assay kit. Briefly, the cell supernatants were taken and centrifuged at 250 x g for 4 min to eliminate cell debris. Then 50 µl of the supernatant was transferred to 96-well microplate and 50 µl of Substrate Mix was added and incubated for 30 min at room temperature, protected from light. After this time, 50 µl of the Stop solution from the kit was added. Absorbance at 490 nm was measured in a Cytation 5 plate reader. 10 µl of the lysis solution (10X) per 100 µL of medium added one hour before the end of the assay was used as LDH release control.

2.16. Determination of TNF-α

TNF-α release in supernatants was measured by ELISA kit (BD Biosciences) according to the manufacturer's instructions.

2.17. Reactive Oxygen Species (ROS) Assay

ROS levels were determined using the fluorescent probe, carboxy-H_2DCFDA. Briefly, cells were seeded at a density of 7.5 x 10^4 per well in a 24-well microplate and grown for 24 h at 37°C. Then, cells were incubated with BS-TA-ARC and irradiated as state in section 2.15. Subsequently, the medium was removed, and cells were incubated with 13 µM H_2DCFDA for 30 min at 37°C. After incubation, H_2DCFDA was removed and 300 µl of PBS was added per well. Fluorescence was determined at Ex/Em: ~492–495/517–527nm (excitation wavelength 485 nm ± 20 nm and emission wavelength 530 ± 30) using a Cytation 5 plate reader. A ~2.5 µM H_2O_2 solution incubated for 3 h before adding H_2DCFDA was used as a positive control.

2.18. Apoptosis and Necrosis

Induction of apoptosis/necrosis was determined by fluorescence microscopy by staining with YO-PRO-1 and IP as fluorescent markers for apoptosis and necrosis, respectively. To locate the cell nucleus, the cells were also stained with Hoechst. Cells were seed and treated as state in section 2.17. Once the incubation was finished, the media was discarded, washed once with PBS and 1ml of cold PBS was added. Subsequently, 1 µl of 100 µM YO-PRO-1 and 20 µl of 160 µM Hoechst were added; after 15 min 1 µl of 0.1 mg/ml IP was added and incubated for another 5 min on ice. Cells were washed again with PBS and 1 ml of PBS was left. Immediately, the cells were observed in a Cytation 5 instrument (YO-PRO was observed with the fluorescence cube YFP, PI was observed with the RFP cube, and Hoechst with the DAPI cube). Micrographs were taken at 20X. A positive control for apoptosis was carried out 24 h before the staining by submitting the cells to UV irradiation (254 nm) for 30 min. A positive control for necrosis was carried out by incubating cells with 2.5 mM H_2O_2 in PBS for 3 h before the staining.

2.19. Statistics

Statistical analyses were performed using a one-way ANOVA followed by Dunnett's test, employing Prism 8.0 software (GraphPad, CA, USA). A p-value < 0.05 was considered statistically significant. The significance levels were defined as follows: $p < 0.05$ (*), $p < 0.01$ (**), $p < 0.001$ (***), and $p < 0.0001$ (****); "n.s." denotes non-significant results ($p > 0.05$). Additionally, a Student's *t*-test was conducted, using the same p-value thresholds.

 doi:10.20944/preprints202601.0767.v1

3. Results and Discussion

3.1. Total Archaeolipid Extraction and Analysis

In this study, we employed a binary mixture of EtOAc (aprotic solvent more polar than chloroform) and EtOH (polar protic solvent) to obtain a mixture of TA (NA and PA) from haloarchaeal biomass employing two extraction steps. The first step was the solid–liquid extraction of the concentrated biomass that was disrupted and its components solubilized in an ethyl acetate/ethanol/water mixture (2:1:0.8, v/v/v). In the second a liquid–liquid extraction, of the centrifugation supernatant from the extracted biomass was performed extracting with ethyl acetate and water mixture (2:1, v/v), up to a final ethyl acetate/ethanol/water ratio of 2:1:1 (v/v/v). Phospholipids, proteins and sugar were measured in the organic and aqueous phases of the final biphasic system of both classical BD method and extraction method with BS (Figure 1). The organic phase from the BS method contained significantly higher proportions of phospholipids and sugars compared to the classical BD method; however, protein proportions were similar.

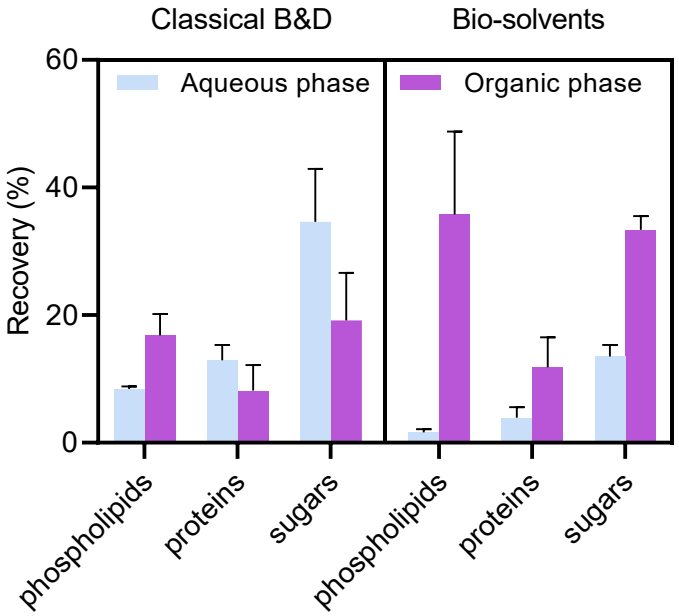

Figure 1. Phospholipids, proteins and sugar quantification into the aqueous and organic phases extracte by the classical Bligh and Dyer (BD) method and by the bio-solvents. Data are expressed as mean ± SD (n=4).

The BS method also rendered a significantly lower phospholipid (PL) yield (135 ± 41.0 mg vs. 192 ± 22.6 mg per 100 g cell paste; $p < 0.001$; $n = 12$), while the two methods yielded comparable amounts of BR (1.1 ± 0.4 mg vs. 1.3 ± 0.3 mg per 100 g; $p > 0.05$). Consequently, the TA extracted by the BS method BS-TA exhibited a slightly higher BR/PL ratio (9.0 vs. 6.8 µg/mg), although this difference did not reach statistical significance. Accordingly, recently it has been reported that EtOAc extracts a higher proportion of neutral lipids than polar lipids (PL) from biomass from several marine fish species [51].

The UV–visible spectrum of BS-TA exhibited the characteristic absorption features of BR, with maxima at 455, 490, and 525 nm, as well as two additional peaks associated with cis isomer configurations, observed at 365 and 380 nm [52] (Figure 2A).

The ESI-MS spectrum of BS-TA in negative mode showed five strong peaks at m/z 449 (phosphatidylglycerophosphate methyl ester, PGP-Me, as a bicharged ion), m/z 484 (loss of a phytanyl chain (280 Da) from cardiolipin bisphosphatidyl glycerol, BPG), m/z 805 (phosphatidylglycerol, PG), m/z 899 (phosphatidylglycerophosphate methyl ester, PGP-Me) and m/z

 doi:10.20944/preprints202601.0767.v1

1055 m/z (sulfated mannosyl glucosyl diether (S-DGD) as recently was reported for BD-TA [22] (Figure 2B). In contrast, the peak at m/z 884, corresponding to phosphatidylglycerosulfate (PGS), was not detected. Notably, this peak was also absent in PA extracted from H. tebenquichense [53]. The signal corresponding to archaeal cardiolipin (bisphosphatidylglycerol, BPG), expected at m/z 760 as a doubly charged ion, was neither detected.

The ESI-MS spectrum of BS-TA in positive mode showed five strong protonated peaks at m/z 517 ([M+H]$^+$ a C_{37}-apocarotenone/apocarotenol derivative produced by oxidative cleavage of C_{40} carotenoid), m/z 561 (represents the glycerol-ether core after losing a portion of a larger polar headgroup), m/z 591 (a C_{40} carotenoid (e.g., apocarotenoid or oxygenated C_{40}) with 3 oxygens), m/z 675 ([tetra anhydro BR-H]+) and m/z 749 (could be an oxidized/oxygenated or esterified derivative of BR (m/z 741) since the MS/MS confirm that the peak corresponded to BR) (Figure 2C). These last two reported for BD-TA [22]. Peaks of lower intensity in BS-TA were also observed at m/z 413 ([dihydrosqualene-H]+) and m/z 597 ([astaxanthin-H]+) as recently reported [22].

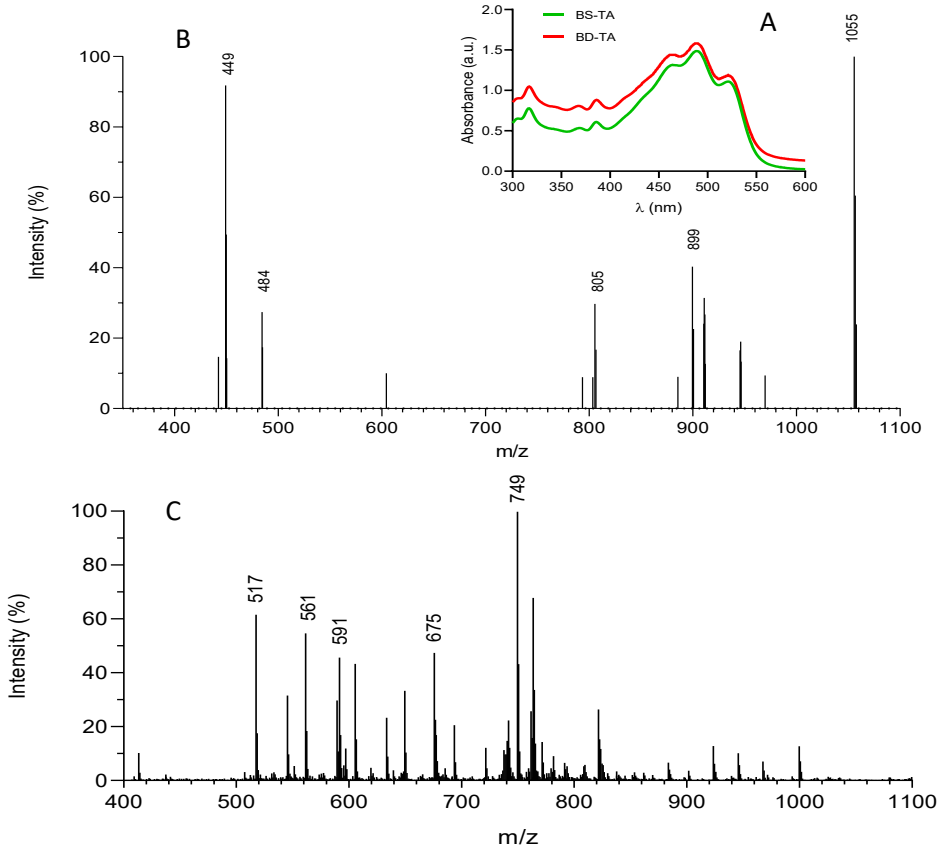

Figure 2. Characterization of total archaeolipids (TA) from *H. tebenquichense* extracted by bio-solvents. (A) UV-vis spectra; (B) Electrospray ionization–mass spectrometry (ESI-MS) analysis in negative ion mode and (C) in positive ion mode.

The IC50 of BS-TA was 2.4 ± 0.2 μg/ml, reflecting its higher BR content and subsequent higher antioxidant activity, in comparison to the IC50 of 5.7 ± 1.3 μg/ml from BD-TA, slightly lower than the reference antioxidant Trolox (IC50 7.1 ± 0.9 μg/ml).

Importantly, to optimize solvent reuse and protein recovery, the two-phase system can be further processed as proposed by Mussagy et al. (2020) [29]. The organic top phase can undergo evaporation to reclaim EtOAc. The aqueous bottom phase can be either recycled for further extraction or treated to extract proteins; the latter involves adding fresh EtOH (70–90% v/v) and incubating at 4°C to -20°C to induce precipitation.

3.2. Structural Characterization of BS-TA-ARC

 doi:10.20944/preprints202601.0767.v1

The structural features of BS-TA-ARC and BD-TA-ARC are shown in Table 1. BS-TA-ARC were larger and with higher PDI that BD-TA-ARC but exhibited negative and comparable ζ potential. The BS-TA-ARC bilayer were more ordered, tightly packed, less hydrated (higher GP) and slightly less fluid (inversely correlated to FA) than the BD-TA-ARC bilayers. This means that ARC membrane prepared with BS-TA has become stiffer and its internal environment has become less polar due to a decrease in water content with higher microviscosity compared with ARC prepared with BD-TA. All these changes could be ascribed to the higher BR content of BS-TA-ARC, as already reported [19].

Table 1. Structural features of TA-ARC. Values of Z average, polydispersity index (Pdi), bacterioruberin/phospholipid (BR/PL), fluorescence anisotropy (FA) and generalized polarization (GP) are expressed as mean ± standard deviation (SD) (n = 3). Statistical significance of FA and GP compared to BD-TA-ARC was determined using a one-way ANOVA followed by Dunnet's test, *p < 0.05; ** p < 0.01.

Formulation	PL (mg/ml)	Z Average (nm ± SD)	Pdi ± SD	BR/PL (μg/mg ± SD)	ζ Potential (mV ± SD)	FA	GP
BD-TA-ARC	18.3 ± 1.6	297 ± 74.2	0.57 ± 0.13	6.7 ± 0.9	- 41.6 ± 5	0.27 ± 0.04	-0.29 ± 0.07
BS-TA-ARC	18.9 ± 3.2	406 ± 137	0.63 ± 0.13	8.2 ± 1.0	- 38.2 ± 5.4	0.29 ± 0.05*	-0.12 ± 0.02**

Characteristic peaks of BR were observed in Raman spectra of both BS-TA-ARC and BD-TA-ARC at 868 cm- 1 (COC ring mode of the sugar), 956 cm- 1 (CH3 rocking in-plane), and 1002 cm- 1 (C–CH deformation), 1000 (C═CH deformation), 1151 (C—C stretching mode) and 1509-5 cm^{-1} (C═C stretching mode) (Figure 3).

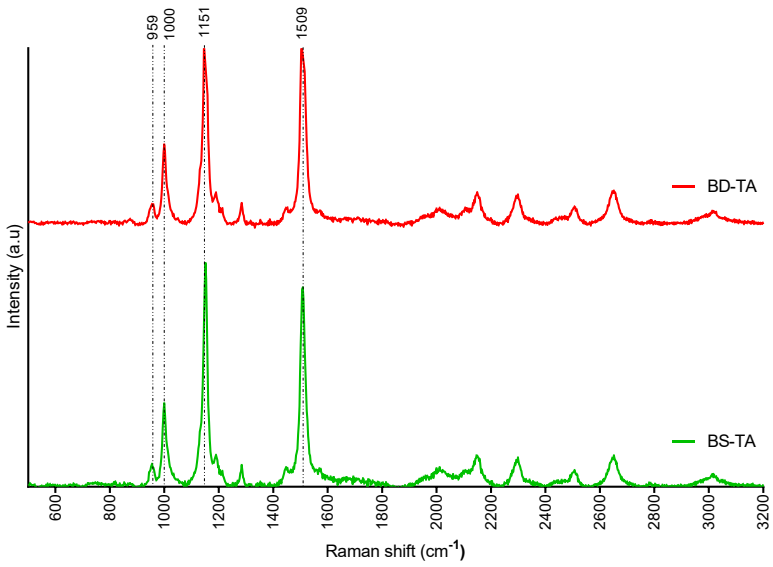

Figure 3. RAMAN spectra of BD-TA and BS-TA of *H. tebenquichense.*

After 2 months of storage at 4 ◦C in dark conditions, AM-TA-ARC and BD-TA-ARC maintained stable colloidal parameters, including size, PDI, and ζ potential (Figure 4).

 doi:10.20944/preprints202601.0767.v1

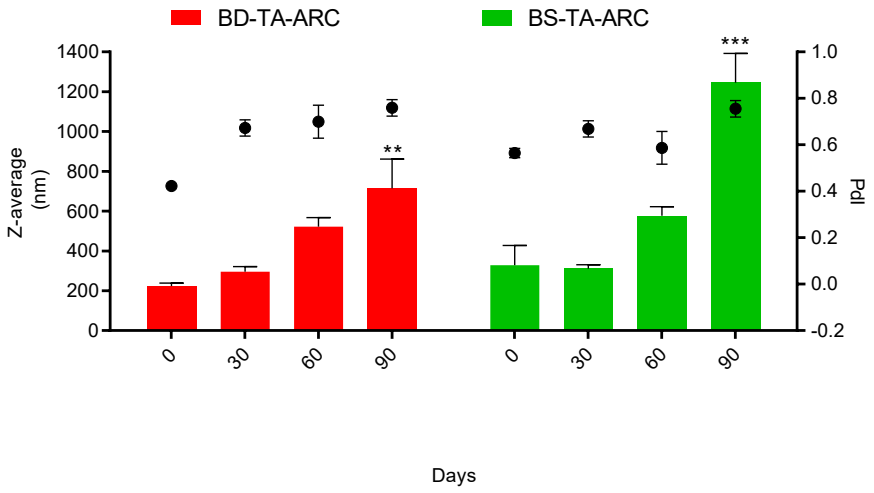

Figure 4. Colloidal stability under storage of BD-TA-ARC and BS-TA-ARC. Data are expressed as mean ± SD (n = 3).

3.3. Cellular Toxicity and Uptake of AM-TA-ARC

The effect of BS-TA-ARC on HaCaT cell viability was first determined after 24 h. Because viability remained high at 1 mg/mL (75%, Figure 5), a concentration of 500 µg/mL was utilized for further experiments as a non-cytotoxic dose. Subsequent fluorescence microscopy revealed that Rh-PE-labeled BS-TA-ARC was internalized by the cells in a time-dependent fashion (Figure 6).

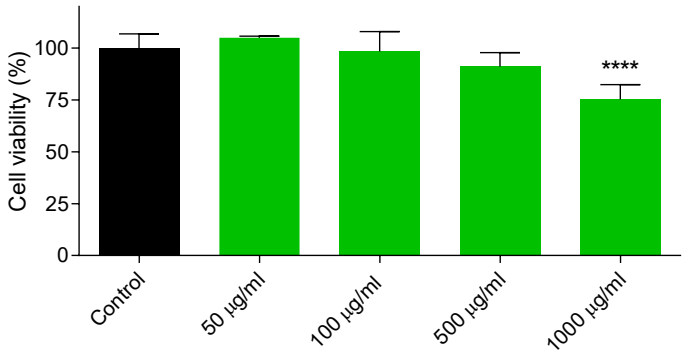

Figure 5. Cytotoxicity of HaCaT cells upon 24 h incubation with BS-TA-ARC Data are expressed as mean ± SD (n = 3).

 doi:10.20944/preprints202601.0767.v1

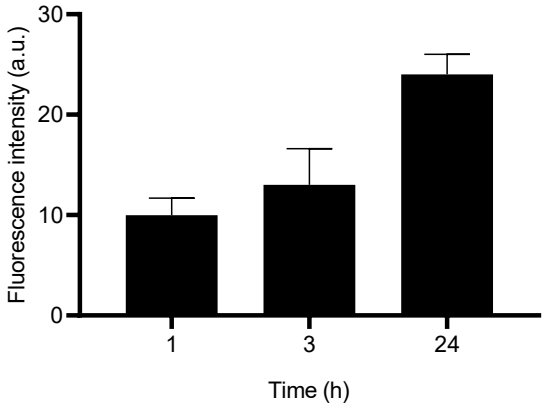

Figure 6. Uptake of BS-TA-ARC by HaCaT cells. Data are expressed as mean ± SD (n = 3).

3.4. Impact of UVB Irradiation on Cell Viability

UVB irradiation significantly decreased HaCaT cell viability in a time-dependent manner (Figure 7). An *LD*50 of 270 mJ/cm^2 was achieved after 20 minutes of exposure (10 cm distance). While standard genotoxicity models often utilize lower doses (10–30 mJ/cm^2) for sublethal damage, the higher dose observed here is consistent with acute irradiation protocols known to induce programmed cell death [54]. Differences between studies likely reflect lamp spectrum, irradiance, dosimetry, and culture conditions.

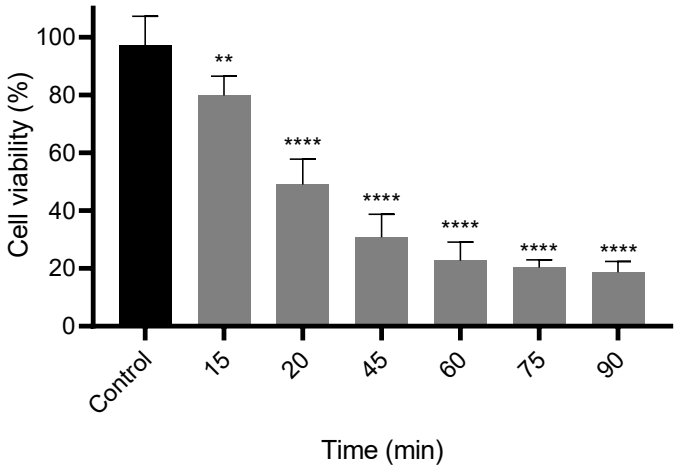

Figure 7. Effects of UVB radiation time on the viability in HaCaT cells. The control group consisted of cells cultured in medium only. Data are expressed as mean ± SD (n = 3).

3.5. Photoprotective Activity of AM-TA-ARC

The photoprotective effect of BS-TA-ARC pretreatment against UVB-induced damage is illustrated in Figure 8. Pretreatment significantly mitigated cytotoxicity, as evidenced by improved metabolic activity (MTT assay; Figure 8A) and reduced membrane damage (LDH release; Figure 8B). Furthermore, BS-TA-ARC significantly attenuated the intracellular ROS production (Figure 8C) and TNF-α secretion (Figure 8D) typically elicited by UVB exposure.

 doi:10.20944/preprints202601.0767.v1

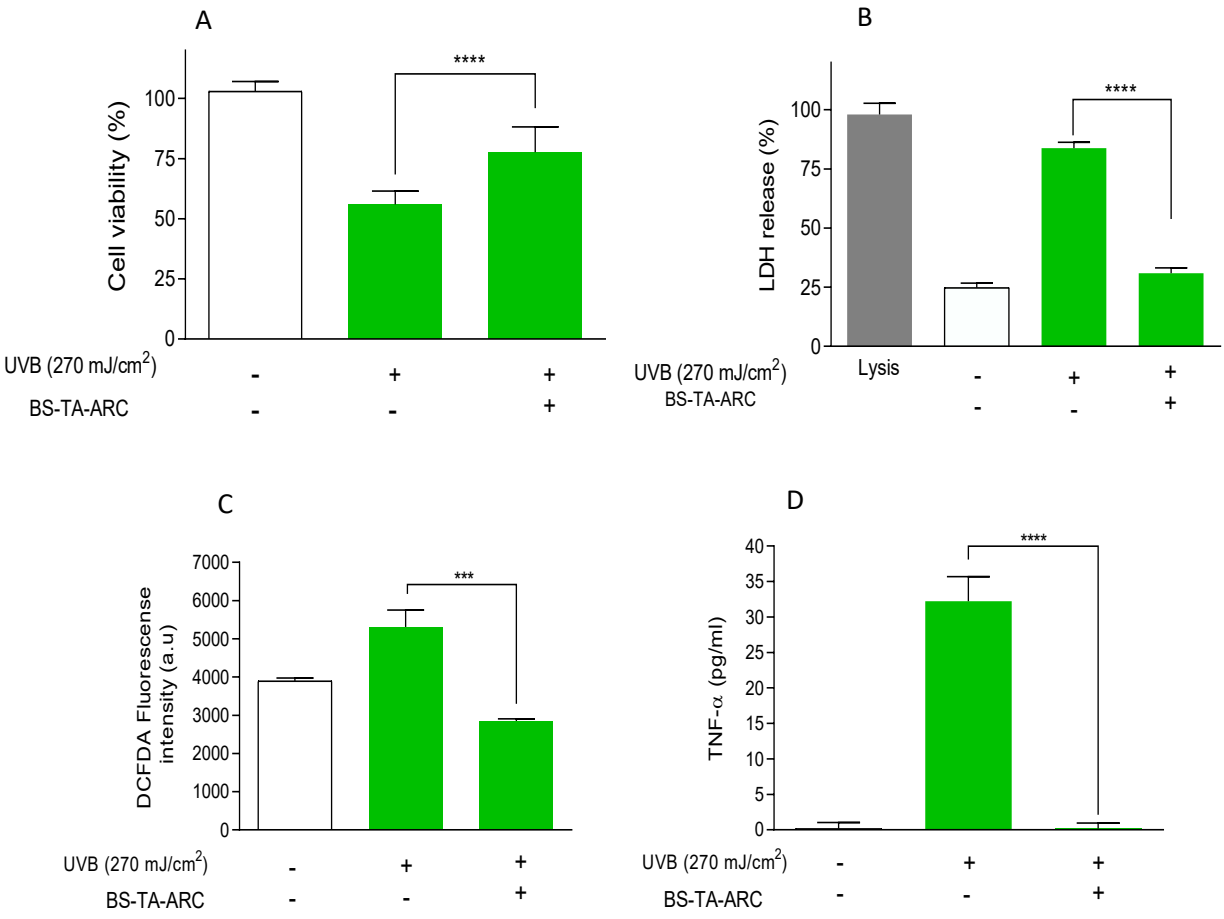

Figure 8. Photoprotective effects of BS-TA-ARC on UVB-irradiated HaCaT cells. A) Cytotoxicity measured by MTT; B) LDH relase; C) Intracellular ROS generation and D) TNF-α release. Data are expressed as mean ± SD (n = 3).

UVB irradiation significantly increased the percentage of apoptotic cells (Figure 9 A and B). However, pretreatment with AM-TA-ARC markedly attenuated UVB-induced apoptosis, as shown by a significant reduction in the apoptotic cell population.

Carotenoids such as β-carotene, lycopene and astaxanthin provide protection against UV radiation by scavenging ROS and modulating oxidative stress responsive signal pathways, including MAPK (mitogen-activated protein kinase, culminating in expression of matrix metalloproteinases, upregulation of expression of inflammatory factors), Nrf2 (nuclear factor erythroid 2-related factor 2 a master regulatory system for cellular redox homeostasis), and NF-κB (nuclear factor kappa-B) [40]. Previous studies have demonstrated that BR dissolved in DMSO can modulate the Nrf2 pathway [55]. After 24 h of internalization by HaCaT keratinocytes, BS-TA-ARC significantly reduced UVB-induced cytotoxicity and markedly reduced levels of intracellular ROS compared with non-treated controls. Both facts suggested that BS-TA-ARC stabilized mitochondrial function, probably preventing lipid peroxidation, two major pathways involved in UVB-induced cell death [56]. Accordingly, Gonzalez Epelboim et al., 2025 [22] showed that ARC prepared with BD-TA protect mitochondria of human lung adenocarcinoma epithelial cell line A549. The reduction in UVB-induced release of pro-inflammatory cytokines and apoptosis, suggests that BS-TA-ARC inhibited key signalling cascades involved in photo-inflammation, and intrinsic apoptotic pathways, contributing to preserve mitochondrial function. The dual reduction in ROS and TNF-α suggests activation of cytoprotective pathways such as Nrf2 and inhibition of NF-κB signalling, mechanisms consistent with previously reported antioxidant carotenoid activity [57]. This protective effect aligns with reports that antioxidants including astaxanthin can stabilize mitochondrial membrane potential

 doi:10.20944/preprints202601.0767.v1

and suppress the activation of caspase-dependent apoptosis following UV exposure [58,59]. Together, these facts indicate a comprehensive cytoprotective mechanism mediated by BS-TA-ARC.

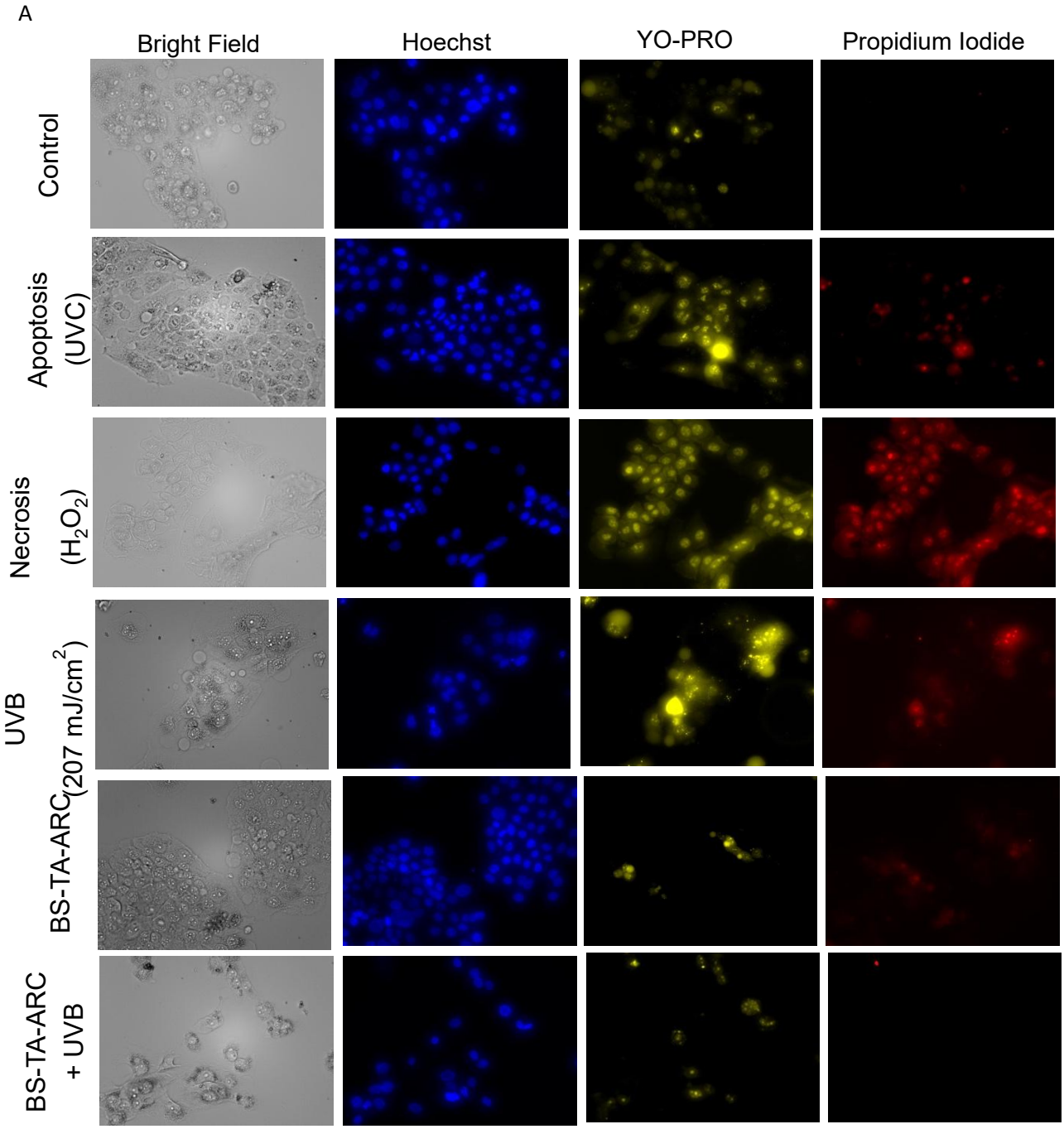

 doi:10.20944/preprints202601.0767.v1

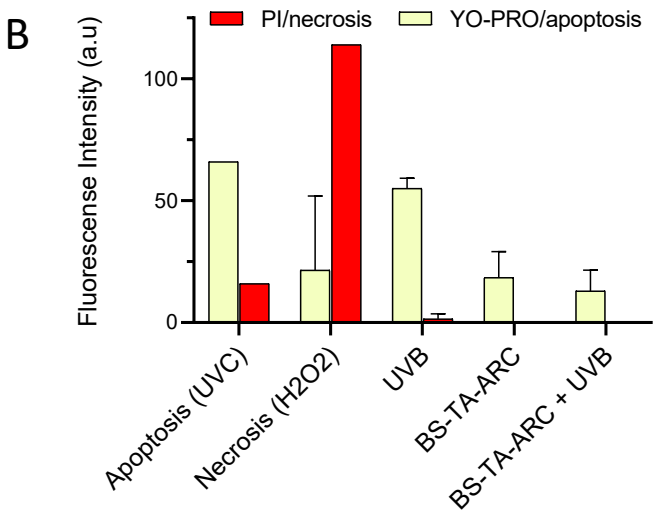

Figure 9. A) Representative HaCaT cells microscopy images after incubation BS-TA-ARC and UVB irradiation. Bright field, Hoechst staining (blue nuclei), YO-PRO staining (green, for apoptotic cells), PI staining (red, for necrotic cells). Magnification 20 X. B) Fluorescence intensity of PI and YO-PRO.

4. Conclusions

This work demonstrates that archaeosomes prepared from total archaeolipids extracted with an ethyl acetate–ethanol mixture are efficient carriers for bacterioruberin, enabling its effective internalization by HaCaT keratinocytes. The bacterioruberin-loaded archaeosomes provided significant protection against UVB-induced cytotoxicity, oxidative stress, inflammation, and apoptosis. These effects likely result from a combination of direct radical-scavenging activity, stabilization of mitochondrial function, and modulation of redox-sensitive signalling pathways. The use of archaeal lipids as a natural, stable matrix offers a sustainable and biocompatible strategy for developing next-generation topical formulations aimed at photoprotection and skin health. Together, these findings highlight the potential of bacterioruberin-loaded archaeosomes as multifunctional bioinspired nanocarriers for dermatological and cosmetic applications.

Author Contributions: Conceptualization, M.J.M; Methodology, Y.R.S., V.R.D.G.E, G.A. and L.H.H.; Software, M.J.M.; Validation and Formal analysis, M.J.M; Investigation, Y.R.S., V.R.D.G.E., and L.H.H.; Resources, M.J.M. and E.L.R.; Data Curation, L.H.H., E.L.R. and M.J.M.; Writing—Original Draft Preparation, Y.R.S. and M.J.M.; Writing—Review and Editing, M.J.M., and E.L.R.; Visualization and Supervision, M.J.M.; Project Administration, M.J.M.; Funding Acquisition, M.J.M. and E.L.R. All authors have read and agreed to the published version of the manuscript.

Funding: This research was funded by Agencia Nacional de Promoción Científica y Tecnológica (ANPCYT, PICT Start up 2016-0019), the National Council for Scientific and Technological Research (CONICET, PIP 2021–2023 N° 11220200102694CO), and the Secretaría de Investigaciones, Universidad Nacional de Quilmes (Programa de Nanomedicinas-2).

Data Availability Statement: The data presented in this study are available upon request from the corresponding author.

Acknowledgments: YRS and VRDGE are doctoral fellows of CONICET LHH, ELR and MJM are members of the Research Career Program from CONICET. During the preparation of this manuscript the authors used ChatGPT to assist in rephrasing certain sentences. The authors have reviewed and edited the output and take full responsibility for the content of this publication.

Conflicts of Interest: The authors declare no conflicts of interest.

 doi:10.20944/preprints202601.0767.v1

References

1. Morilla, M.J.; Romero, E.L. Ether lipids from archaea in nano-drug delivery. *Int J Pharm*. **2023**, *634*, 122632.
2. Jain, S.; Caforio, A.; Driessen, A.J. Biosynthesis of archaeal membrane ether lipids. *Front Microbiol*. **2014,** *5*, 641.
3. Villanueva, L.; Schouten, S.; Damsté, J.S.S. Phylogenomic analysis of lipid biosynthetic genes of Archaea shed light on the lipid divide. *Environ Microbiol*. **2017**, *19*, 54–69.
4. Caforio, A.; Driessen, A.J.M. Archaeal phospholipids: structural properties and biosynthesis. *Biochim Biophys Acta Mol Cell Biol Lipids* **2017**, *1862*, 1325–1339.
5. Matsumi, R.; Atomi, H.; Driessen, A.J.; van der Oost, J. Isoprenoid biosynthesis in Archaea--biochemical and evolutionary implications. *Res Microbiol*. **2011**, *162(1)*, 39-52.
6. Chong, P.L.G.; Chang, A.; Yu, A.; Mammedova, A. Vesicular and planar membranes of archaeal lipids: unusual physical properties and biomedical applications. *Int J Mol Sci.* **2022**, *23*, 7616.
7. Lizama, C.; Romero-Parra, J.; Andrade, D.; Riveros, F.; Bórquez, J.; Ahmed, S.; Venegas-Salas, L.; Cabalín, C.; Simirgiotis, M.J. Analysis of Carotenoids in Haloarchaea Species from Atacama Saline Lakes by High Resolution UHPLC-Q-Orbitrap-Mass Spectrometry: Antioxidant Potential and Biological Effect on Cell Viability. *Antioxidants* **2021,** *10*, 1230.
8. Mandelli, F.; Miranda, V.S.; Rodrigues, E.; Mercadante, A.Z. Identification of carotenoids with high antioxidant capacity produced by extremophile microorganisms. *World J Microbiol Biotechnol.* **2012**, *28*(4), 1781-90.
9. Shahmohammadi, H.R.; Asgarani, E.; Terato, H.; Saito, T.; Ohyama, Y.; Gekko, K.; Yamamoto, O.; Ide, H. Protective Roles of Bacterioruberin and Intracellular KCl in the Resistance of Halobacterium Salinarium against DNA-Damaging Agents. *J. Radiat. Res.* **1998**, *39*, 251–262.
10. Fong, N.J.; Burgess, M.L.; Barrow, K.D.; Glenn, D.R. Carotenoid accumulation in the psychrotrophic bacterium *Arthrobacter agilis* in response to thermal and salt stress. *Appl Microbiol Biotechnol.* **2001**, *56*(5–6), 750–6.
11. Martínez-Espinosa, R.M. Bacterioruberin (C50 carotenoid): nutritional and biomedical potential. *Nutrients* **2025**, *17*, 3899.
12. Ma, Y.; Sun, Z.; Yang, H.; Xie, W.; Song, M.; Zhang, B.; Sui, L. The biosynthesis mechanism of bacterioruberin in halophilic archaea revealed by genome and transcriptome analysis. *Appl Environ Microbiol*. **2024**, *90*(7), e0054024.
13. Giani, M.; Martínez-Espinosa, R.M. Carotenoids as a protection mechanism against oxidative stress in *Haloferax mediterranei*. *Antioxidants* **2020**, *9*, 1060
14. Caimi, A.T.; Parra, F.; de Farias, M.A.; Portugal, R.V.; Perez, A.P.; Romero, E.L.; Morilla, M.J. Topical vaccination with super-stable ready to use nanovesicles. *Colloids Surf B: Biointerfaces* **2016**, *152*, 114-123.
15. Altube, M.J.; Selzer, S.M.; de Farias, M.A.; Portugal, R.V.; Morilla, M.J.; Romero, E.L. Surviving nebulization-induced stress: dexamethasone in pH-sensitive archaeosomes. *Nanomedicine (Lond)* **2016**, *11*(16), 2103-17.
16. Higa, L.H.; Schilrreff, P.; Briski, A.M.; Jerez, H.E.; de Farias, M.A.; Villares Portugal, R.; Romero, E.L.; Morilla, M.J. Bacterioruberin from Haloarchaea plus dexamethasone in ultra-small macrophage-targeted nanoparticles as potential intestinal repairing agent. *Colloids Surf B Biointerfaces.* **2020**, *191*, 110961.
17. Schilrreff, P.; Simioni, Y.R.; Jerez, H.E.; Caimi, A.T.; de Farias, M.A.; Villares Portugal, R.; Romero, E.L.; Morilla, M.J. Superoxide dismutase in nanoarchaeosomes for targeted delivery to inflammatory macrophages. *Colloids Surf B Biointerfaces*. **2019**, *179*, 479-487.
18. Charó, N.; Jerez, H.; Tatti, S.; Romero, E.L.; Schattner, M. The Anti-Inflammatory Effect of Nanoarchaeosomes on Human Endothelial Cells. *Pharmaceutics* **2022**, *14*, 736.
19. Caimi, A.T.; Yasynska, O., Rivas Rojas, P.C.; Romero, E.L.; Morilla, M.J. Improved stability and biological activity of bacterioruberin in nanovesicles. *J Drug Deliv Sci Technol* **2022**, *77*, 103896.
20. Kates, M. Membrane lipids of archaea. *Biochem Soc Trans*. **1993**, *21*, 100–104.
21. Angelini, R.; Corral, P.; Mavridou, D.A.I.; Texeira, M., Ventosa, A. Lipidomics of haloarchaea. *Appl Environ Microbiol* **2012**, *78*(14), 5353–5363.

 doi:10.20944/preprints202601.0767.v1

22. Gonzalez Epelboim, V.R.D.; Lamas, D.G.; Huck-Iriart, C.; Caputo, E.N.; Altube, M.J.; Jerez, H.E.; Simioni, Y.R.; Ghosal, K.; Morilla, M.J.; Higa, L.H.; Romero, E.L. Nebulized Bacterioruberin/Astaxanthin-Loaded Nanovesicles: Antitumoral Activity and Beyond. *Int. J. Mol. Sci.* **2025**, *26*, 8607.
23. https://www.epa.gov/sites/default/files/2016-09/documents/methanol.pdf (accessed on 20 Dec 2025)
24. National Institute for Occupational Safety and Health. (2023). *NIOSH pocket guide to chemical hazards: Methanol*. Centers for Disease Control and Prevention. https://www.cdc.gov/niosh/npg (accessed on 20 Dec 2025)
25. EPA. (2024). *Managing hazardous waste solvents*. U.S. Environmental Protection Agency. https://www.epa.gov/hw
26. Prat, D.; Wells, A.; Hayler, J.; et al. CHEM21 solvent selection guide. *Green Chem*. **2016**, *18*, 288–296.
27. Anastas, P.T.; Warner, J.C. *Green chemistry: theory and practice*. Oxford: Oxford University Press **1998**.
28. Breil, C.; Abert Vian, M.; Zemb, T.; Kunz, W.; Chemat, F. "Bligh and Dyer" and Folch methods for solid-liquid-liquid extraction of lipids from microorganisms. Comprehension of Solvatation mechanisms and towards substitution with alternative solvents. *Int J Mol Sci*. **2017**, *18*(4), 1–21.
29. Mussagy, C.; Santos-Ebinuma, V.C.; Kurnia, K.A.; Dias, A.C.R.V.; Carvalho, P.; Coutinho, J.A.P.; Pereira, J.F.B. Integrative platform for the selective recovery of intracellular carotenoids and lipids from *Rhodotorula glutinis* CCT-2186 yeast using mixtures of bio-based solvents. *Green Chem* **2020**, *23*
30. Marques, F.; Pinho, M.; Guerra, I.M.S.; Conde, T.A.; Silva, J.; Cardoso, H.; Martins, M.; Abreu, M.H.; Cerqueira, M.A.; Domingues, M.R. Unlocking functional lipid ingredients from algae by foodgrade biosolvents and ultrasound-assisted extraction for nutritional applications. *LWT* **2024**, *200*, 116136.
31. Popescu, M.; Iancu, P.; Plesu, V.; Todasca, M.C.; Isopencu, G.O.; Bildea, C.S. Valuable Natural Antioxidant Products Recovered from Tomatoes by Green Extraction. *Molecules* **2022**, *27*, 4191.
32. Prasad, W.; Wani, A.D.; Khamrui, K.; Hussain, S.A.; Khetra, Y. Green solvents, potential alternatives for petroleum based products in food processing industries. *Clean. Chem. Eng*. **2022**, *3*, 100052.
33. Viñas-Ospino, A.; López-Malo, D.; Esteve, M.J.; Frígola, A.; Blesa, J. Green Solvents: Emerging Alternatives for Carotenoid Extraction from Fruit and Vegetable By-Products. *Foods* **2023**, *12*, 863.
34. Tang, X.; Yang, T.; Yu, D.; Xiong, H.; Zhang, S. Current insights and future perspectives of ultraviolet radiation (UV) exposure: Friends and foes to the skin and beyond the skin. *Environ Int.* **2024**, *185*, 108535.
35. Gromkowska-Kępka, K.J.; Puścion-Jakubik, A.; Markiewicz-Żukowska, R.; Socha, K. The impact of ultraviolet radiation on skin photoaging - review of in vitro studies. *J Cosmet Dermatol*. **2021**, *20*(11), 3427-3431.
36. Tanveer, M.A.; Rashid, H.; Tasduq, S.A. Molecular basis of skin photoaging and therapeutic interventions by plant-derived natural product ingredients: A comprehensive review. *Heliyon* **2023**, *9*(3), e13580.
37. Budzianowska, A.; Banaś, K.; Budzianowski, J.; Kikowska, M.; Antioxidants to Defend Healthy and Youthful Skin—Current Trends and Future Directions in Cosmetology. *Applied Sciences* **2025**, *15*(5), 2571.
38. Raszewska-Famielec, M.; Radzikowska-Büchner, E.; Flieger, W. Skin Protection by Carotenoid Pigments. *Int. J. Mol. Sci.* **2024**, *25*, 1431.
39. Catanzaro, E.; Bishayee, A.; Fimognari, C. On a Beam of Light: Photoprotective Activities of the Marine Carotenoids Astaxanthin and Fucoxanthin in Suppression of Inflammation and Cancer. *Mar. Drugs* **2020**, *18*, 544.
40. Ma, Y.; Li, C.; Su, W.; Sun, Z.; Gao, S.; Xie, W.; Zhang, B.; Sui, L. Carotenoids in Skin Photoaging: Unveiling Protective Effects, Molecular Insights, and Safety and Bioavailability Frontiers. *Antioxidants* **2025**, *14*(5), 577.
41. Semitsoglou-Tsiapou, S.; Meador, T.B.; Peng, B.; Aluwihare, L. Photochemical (UV–Vis/H2O2) Degradation of Carotenoids: Kinetics and Molecular End Products. *Chemosphere* **2022**, *286*, 131697.
42. Behzadi, S.; Serpooshan, V.; Tao, W.; Hamaly, M.A.; Alkawareek, M.Y.; Dreaden, E.C.; Brown, D.; Alkilany, A.M.; Farokhzad, O.C.; Mahmoudi, M. Cellular uptake of nanoparticles: journey inside the cell. *Chem Soc Rev*. **2017**, *46*(14), 4218-4244.
43. Lima, S.G.M.; Freire, M.C.L.C.; Oliveira, V.dS.; Solisio, C.; Converti, A.; de Lima, Á.A.N. Astaxanthin Delivery Systems for Skin Application: A Review. *Mar. Drugs* **2021**, *19*, 511.
44. Villalaín, J. Location and dynamics of astaxanthin in the membrane. *Biochim Biophys Acta (BBA)-Biomembranes*. **2025**, *270*, 105512. doi: 10.1016/j.chemphyslip.2025.105512

 doi:10.20944/preprints202601.0767.v1

45. Flegler, A.; Lipski, A. The C_{50} carotenoid bacterioruberin regulates membrane fluidity in pink-pigmented Arthrobacter species. *Arch Microbiol* **2021**, *204*(1), 70.
46. Ihara, K.; Watanabe, S.; Tamura, T. Haloarcula argentinensis sp. nov. and Haloarcula mukohataei sp. nov., two new extremely halophilic archaea collected in Argentina. *Int J Syst Bacteriol*. **1997**, *47*(1), 73-7.
47. Bottcher, C.J.F.; Van Gent, C.M.; Pries, C.A. Rapid and Sensitive Sub-Micro Phosphorus Determination. *Anal. Chim. Acta* **1961**, *24*, 203–204
48. Dubois, M., Gilles, K.A., Hamilton, J.K., Rebers, P.A., Smith, F. Colorimetric method for determination of sugars and related substances. *Anal. Chem*. **1956**, *28*, 350– 356
49. Britton, G.; Liaaen-Jensen, S.; Pfander, H. *Carotenoids.* Basel: Birkhäuser, **2004**.
50. Jimenez-Escrig, A.; Jimenez-Jimenez, I.; Sanchez-Moreno, C.; Saura-Calixto, F. Evaluation of Free Radical Scavenging of Dietary Carotenoids by the Stable Radical 2,2-Diphenyl-1-Picrylhydrazyl. *J. Sci. Food Agric*. **2000**, 80, 1686–1690.
51. Wang, Y.; Eilertsen, K.E.; Elvevoll, E.O.; Walquist, M.J. Assessing the efficiency of ethyl acetate for lipid extraction as an alternative to the Folch method. *J Am Oil Chem Soc*. **2025**, *102*, 871–883.
52. Naziri, D.; Hamidi, M.; Hassanzadeh, S.; Tarhriz, V.; Zanjani, B.M.; Nazemyieh, H.; Hejazi, M.A.; Hejazi, M.S. Analysis of Carotenoid Production by Halorubrum Sp. TBZ126; an Extremely Halophilic Archeon from Urmia Lake. *Adv. Pharm. Bull*. **2013**, *4*, 61.
53. Gonzalez, R.O.; Higa, L.H.; Cutrullis, R.A.; Bilen, M.; Morelli, I.; Roncaglia, D.I.; Corral, R.S.; Morilla, M.J.; Petray, P.B.; Romero, E.L. Archaeosomes made of Halorubrum tebenquichense total polar lipids: a new source of adjuvancy. *BMC Biotechnol*. **2009**, *9*, 71.
54. Gag, O.; Dinu, Ș.; Manea, H.; Marcovici, I.; Pînzaru, I.; Popovici, R.; Crăiniceanu, Z.; Gyori, Z; Iovănescu, G.; Chiriac, S. UVA/UVB Irradiation Exerts a Distinct Phototoxic Effect on Human Keratinocytes Compared to Human Malignant Melanoma Cells. *Life (Basel)* **2023**, *13*(5), 1144.
55. Ávila-Román, J.; Gómez- Villegas, P.; de Carvalho, C.C.C.R.; Vigara, J.; Motilva, V.; León, R.; Talero, E. Up-Regulation of the Nrf2/HO-1 Antioxidant Pathway in Macrophages by an Extract from a New Halophilic Archaea Isolated in Odiel Saltworks. *Antioxidants* **2023**, *12*, 1080.
56. Yuan, X.; Li, H.; Lee, J.S.; Lee, D.H. Role of Mitochondrial Dysfunction in UV-Induced Photoaging and Skin Cancers. *Exp Dermatol* **2025**, *34*, e70114.
57. Garcia-Mouronte, E.; Pérez-González, L.A.; Naharro-Rodriguez, J.; Fernández Guarino, M. Understanding Active Photoprotection: DNA-Repair Enzymes and Antioxidants. *Life (Basel)* **2024**, *4*(7), 822.
58. Mohan, M.; Taneja, T.K.; Sahdev, S.; Mohareer, K.; Begum, R.; Athar, M.; Sah, N.K.; Hasnain, S.E. Antioxidants prevent UV-induced apoptosis by inhibiting mitochondrial cytochrome c release and caspase activation in Spodoptera frugiperda (Sf9) cells. *Cell Biol Int*. **2003**, *27*(6), 483-90.
59. Baburina, Y.; Lomovsky, A.; Lomovskaya, Y.; Sotnikov, R.; Sotnikova, L.; Krestinina, O. Mitochondrial Protection by Astaxanthin Reduces Toxicity Caused by H_2O_2 and Doxorubicin in Human Cardiomyocytes. *Cells* **2025**, *14*(22), 1772. doi: 10.3390/cells14221772